Lower bound on the electroweak wall velocity from hydrodynamic instability

Lower bound on the electroweak wall velocity from hydrodynamic instability

Ariel Mégevand, Federico Agustín Membiela and Alejandro D. Sánchez

IFIMAR (CONICET-UNMdP), Departamento de Física,
Facultad de Ciencias Exactas y Naturales,
Universidad Nacional de Mar del Plata, Deán Funes (7600) 3350 Mar del Plata, Argentina

E-mail: megevand@mdp.edu.ar, membiela@mdp.edu.ar, sanchez@mdp.edu.ar

Abstract. The subsonic expansion of bubbles in a strongly first-order electroweak phase transition is a convenient scenario for electroweak baryogenesis. For most extensions of the Standard Model, stationary subsonic solutions (i.e., deflagrations) exist for the propagation of phase transition fronts. However, deflagrations are known to be hydrodynamically unstable for wall velocities below a certain critical value. We calculate this critical velocity for several extensions of the Standard Model and compare with an estimation of the wall velocity. In general, we find a region in parameter space which gives stable deflagrations as well as favorable conditions for electroweak baryogenesis.

Contents

1 Introduction

A first-order electroweak phase transition may explain the observed baryon asymmetry of the universe (BAU). Indeed, such a phase transition would provide all the Sakharov conditions, namely, baryon number violation, C and CP violation, and a departure from thermal equilibrium. For a quantitatively successful electroweak baryogenesis (EWB) an extension of the Standard Model (SM) is needed, such that there is enough CP violation as well as a sufficiently strong first-order phase transition. In the standard mechanism for EWB (see [1] for a recent review), the departure from equilibrium acts in two different ways. On the one hand, the expansion of bubbles of the broken-symmetry phase builds up non-equilibrium particle densities in front of the bubble walls. These densities are asymmetric for left handed particles and their antiparticles due to CP violating interactions with the wall. This asymmetry is transported to the unbroken-symmetry phase, where it biases the weak sphaleron processes which violate baryon number. The generated baryon asymmetry reenters the broken-symmetry phase. As a result, the bubble walls leave behind a net baryon number density. On the other hand, before this baryon number density recovers the equilibrium, the baryon number violating processes should be turned off. Otherwise the generated BAU would be washed out. Such a suppression of the sphaleron processes indeed occurs inside the

– 1 –

bubble, as long as the Higgs background field ϕ_b in the broken-symmetry phase satisfies the well known condition

$$\phi_b/T \gtrsim 1, \tag{1.1}$$

where T is the temperature. The ratio ϕ_b/T plays the role of an order parameter, and the condition (1.1) expresses the baryogenesis requirement of a strongly first-order phase transition.

Although for a Higgs mass as large as $125\,\text{GeV}$ the electroweak phase transition is a smooth crossover, many extensions of the SM give strongly first-order phase transitions. Most investigations of EWB concentrate in the value of the order parameter ϕ_b/T and the sources of CP violation for specific models. Since the computation of the velocity v_w of bubble walls is too involved, a specific value is often assumed (typically $v_w = 0.1$) to obtain a result for the BAU.[1] However, the generated BAU has also an important dependence on v_w. Indeed, for very small velocities thermal equilibrium is restored and a small baryon asymmetry is generated. On the other hand, if the wall velocity is too large the diffusion of left-handed density perturbations is not efficient, and the resulting baryon number density is again small. In other words, a departure from equilibrium is needed, but such a departure should not be too strong. As a consequence, the generated baryon asymmetry has a maximum for a certain wall velocity $v_w = v_{\text{peak}}$. The value of v_{peak} depends on the time scales associated to particle diffusion and baryon number violation, and is in general in the range $10^{-2} < v_{\text{peak}} < 10^{-1}$ (see, e.g., [3–5]). A sizeable BAU is more easily obtained if v_w is close to v_{peak}. Moreover, any model which gives supersonic velocities is in conflict with the standard EWB mechanism [6].

Subsonic wall velocities are possible due to the friction with the plasma, which generally causes the walls to reach a terminal velocity. This velocity is given by the balance between the driving force, which depends on the pressure in the two phases, and the friction force, which depends on the microscopic interactions of the bubble wall with plasma particles. The driving force is very sensitive to hydrodynamics. As a consequence of non-linear hydrodynamics, there are different kinds of stationary solutions for the propagation of the wall [7]. The solutions which can be realized in a cosmological phase transition (see, e.g., [8–14]) are *weak deflagrations*, which are subsonic, *Jouguet deflagrations*, which are supersonic, and *Jouguet or weak detonations*, which are supersonic too. Hence, the case of interest for baryogenesis is that of weak deflagrations.

It is well known that the stationary propagation of a weak deflagration front may be unstable [7]. For the case of a relativistic equation of state, the stability of deflagrations was first studied in ref. [15]. The result was that deflagrations are always unstable under perturbations above a certain wavelength. This analysis was improved in ref. [16]. The main improvement was to take into account the dependence of the stationary velocity on the temperature. The main result of ref. [16] was that the deflagration is stable for wall velocities above a certain critical value v_{crit}. Numerical simulations [17] agree with such a stabilization. In ref. [18], the results of [16] were improved by taking into account temperature fluctuations on both sides of the wall, as well as the fact that the reheating due to the release of latent heat depends on the wall velocity. For small amounts of supercooling, the results of ref. [18] agree with those of ref. [16].

In ref. [16], the stability analysis was applied to the electroweak phase transition for the minimal Standard Model with unrealistic values of the Higgs mass, which gives a strong

---

[1]It is worth mentioning that, in contrast, for the generation of gravitational waves higher velocities are preferable, since the collisions of faster walls produce gravitational waves of higher intensity (see, e.g., [2]). As a consequence, a supersonic wall velocity is generally assumed.

enough phase transition for EWB. For Higgs masses higher than $m_H = 40\,\text{GeV}$, the critical velocity below which deflagrations are unstable was found to be $v_{\text{crit}} \lesssim 0.07$. This result was compared with the wall velocity calculations [19, 20], which gave $v_w \gtrsim 0.1$. Therefore, the result of ref. [16] indicated that the electroweak deflagration is stable. However, both v_w and v_{crit} depend on the model and should be recalculated for each extension of the SM.

The calculation of v_w is more involved than that of v_{crit} and depends on more details of the model. Indeed, the value of the critical velocity depends only on thermodynamical parameters which can be derived from the free energy density. In contrast, the actual value of the stationary velocity depends (besides thermodynamics and hydrodynamics) on the friction of the wall with the plasma. The computation of the friction force involves considering Boltzmann equations for the out-of-equilibrium particle densities in front of the wall. For the SM, a thorough calculation (including reheating effects) [21] gave wall velocities in the range $0.36 < v_w < 0.44$ (for $0 < m_H < 90\,\text{GeV}$). A similar calculation for the Minimal Supersymmetric Standard Model (MSSM) [22] gave smaller velocities, $v_w = (5\text{–}10) \times 10^{-2}$, due to the larger particle content of this model (essentially, due to the contribution of top squarks). To our knowledge, these two results constitute the only detailed microphysics calculations for specific models. The reason for this is the difficulty of computing the collision terms for the Boltzmann equations. In spite of this, many investigations of the friction were performed. In particular, a study of the overdamped evolution of gauge fields [23] showed that infrared boson excitations generally increase the friction and, consequently, cause smaller wall velocities than previous studies. In particular, for the SM the estimated wall velocity was $v_w \lesssim 0.01$ for $m_H \simeq 80\,\text{GeV}$ and $v_w \simeq 0.1$ for $m_H \simeq 45\,\text{GeV}$.

In this paper we shall investigate the possible instability of the electroweak wall velocity for several extensions of the SM. The main motivation for this is the fact that the deflagration instability may affect the baryogenesis scenario. Indeed, notice that the value of v_{crit} obtained in ref. [16] lies within the optimal range for EWB. Moreover, given the general uncertainties and large errors in the estimations of v_w, the value of v_{crit}, which is much easier to calculate, provides a lower bound for v_w which may be important to constrain baryogenesis. It is worth mentioning also that an instability of the stationary wall propagation may have several cosmological consequences, such as the generation of magnetic fields [24] or gravitational waves [18].

The plan of the paper is the following. In section 2 we review the hydrodynamics of a wall which propagates as a deflagration and we discuss the stability of such a stationary solution as a function of thermodynamic parameters. In section 3 we calculate the critical velocity below which the wall becomes unstable. We consider the electroweak phase transition for several extensions of the Standard Model. We also estimate the wall velocity for each model in order to study the stability as a function of the parameters. In section 4 we discuss on the possible consequences of the instability. Finally, in section 5 we summarize our conclusions. Details of the calculation of the phase transition dynamics are contained in appendix A. Further discussion on the critical velocity as well as a fit can be found in appendix B.

2 Stationary wall propagation and hydrodynamic stability

2.1 First-order electroweak phase transition

The relevant quantity describing the phase transition is the free energy density or finite-temperature effective potential[2] $\mathcal{F}(\phi, T)$. At a given temperature T, the minima of $\mathcal{F}$ give

---

[2]In this work we shall only consider models which can be described (at least, approximately) by a single Higgs field ϕ.

the possible thermal expectation values of the Higgs field ϕ, which determine the different phases. For the electroweak theory, we have a phase transition from the symmetric phase to the broken-symmetry phase at a critical temperature $T_c \sim 100\,\mathrm{GeV}$. In the minimal SM, the electroweak phase transition is just a smooth crossover. In section 3 we shall consider several extensions of the SM for which the electroweak phase transition is first-order.

For a first-order phase transition, there is a range of temperatures around T_c for which the effective potential has two minima separated by a barrier. For $T > T_c$ the symmetric minimum $\phi = 0$ is the absolute minimum of $\mathcal{F}(\phi, T)$, while for $T < T_c$ the absolute minimum has a nonvanishing value $\phi_b(T)$. We shall use subindexes u and b for the unbroken- and broken-symmetry phase, respectively. These phases are thus characterized by the free energy densities $\mathcal{F}_u(T) = \mathcal{F}(0, T)$ and $\mathcal{F}_b(T) = \mathcal{F}(\phi_b(T), T)$. The critical temperature is given by the equation $\mathcal{F}_u(T_c) = \mathcal{F}_b(T_c)$. The energy density and pressure for each phase are obtained from the free energy density through $\rho(T) = \mathcal{F}(T) - T\mathcal{F}'(T), p(T) = -\mathcal{F}(T)$, where a prime indicates a derivative with respect to the temperature.

A first-order phase transition occurs via the nucleation and expansion of bubbles. As we shall see, the relevant parameters for our calculation will be the latent heat L defined as $L \equiv \rho_u(T_c) - \rho_b(T_c)$, the enthalpy density before the phase transition, $w_u(T_c) = \rho_u(T_c) + p_u(T_c)$, and the nucleation temperature T_n. The latter is the temperature at which bubbles effectively begin to nucleate. We describe its calculation in appendix A. The enthalpy density and latent heat are given by

$$w_u(T_c) = -T_c \mathcal{F}'_u(T_c), \tag{2.1}$$

$$L = T_c \left[\mathcal{F}'_b(T_c) - \mathcal{F}'_u(T_c) \right]. \tag{2.2}$$

After nucleating, bubbles expand due to the higher pressure of the stable phase. In most cases, the bubble walls quickly reach a terminal velocity due to the friction with the plasma. We shall concentrate in such a case. From the time a bubble nucleates to the time their walls collide with other bubbles, the temperature of the plasma varies due to the adiabatic expansion of the universe and due to the release of latent heat. As a consequence, the wall velocity will vary too. We shall use $T = T_n$ as a representative value for the temperature of the phase transition.

2.2 Microphysics and hydrodynamics

The motion of a bubble wall can be derived from the equation for the Higgs field in the plasma (see, e.g., [19–23, 25–28]),

$$\partial_\mu \partial^\mu \phi + \frac{\partial \mathcal{F}(\phi, T)}{\partial \phi} + \sum_i \frac{dm_i^2}{d\phi} \int \frac{d^3 p}{(2\pi)^3 2E_i} \delta f_i = 0, \tag{2.3}$$

with $E_i = \sqrt{\mathbf{p}^2 + m_i^2}$, where m_i are the ϕ-dependent particle masses, δf_i are the deviations of particle densities from equilibrium, and the sum runs over all particle species. The last term gives the friction with the plasma. In order to transform eq. (2.3) into an equation for the bubble wall, the general procedure is to use some approximation or ansatz for the field profile (which is static in the reference frame of the wall) and integrate across the wall. Since the deviations δf_i depend on the wall velocity, the last term in (2.3) gives the friction force F_{fr}, while the second term gives the driving force F_{dr}. Thus, the steady state velocity of a bubble wall is given by the force balance $F_{\mathrm{dr}} = F_{\mathrm{fr}}$ (for a more detailed explanation, see e.g. [29]).

The driving force is relatively easy to calculate. In particular, if the temperature remains constant across the wall, we have $F_{\mathrm{dr}} = p_b(T) - p_u(T)$. On the other hand, the friction is proportional to the departure of the plasma particles from their equilibrium distributions. This departure from equilibrium depends not only on the interaction of the particles with the Higgs field at the wall, but also on the interactions of plasma particles away from the wall. Thus, the calculation involves solving a system of Boltzmann equations for the population densities of the relevant species. The Boltzmann equations include collision terms which must be computed by calculating the scattering rates for all the relevant processes. Such a calculation is often referred to as the *microphysics* calculation.

As already mentioned in section 1, the microphysics calculation is very difficult. In particular, the computation of the collision terms was carried out only for a couple of models and in the non-relativistic (NR) case [21–23]. The result is a friction force of the form $F_{\mathrm{fr}} = \eta_{\mathrm{NR}} v_w$. The friction coefficient η_{NR} is very model dependent, and its calculation involves the use of several approximations. The ultra-relativistic (UR) limit has also been considered [30]. It turns out that this limit is even simpler than the NR case. The result is that the friction saturates for $v_w \to 1$, i.e., the friction force reaches a velocity-independent value $F_{\mathrm{fr}} = \eta_{\mathrm{UR}}$. Intermediate cases are much more difficult to treat. In a recent treatment [31], the friction was considered beyond the small wall velocity regime. However, the deviations from equilibrium were still considered to be small. In particular, the friction force calculated in ref. [31] does not match the UR results of ref. [30].

In order to overcome the difficulties of the microphysics calculation, a phenomenological approach has often been used, which consists in replacing the last term in eq. (2.3) with an effective damping term of the form $u^\mu \partial_\mu \phi$, where $u^\mu = (\gamma, \gamma \mathbf{v})$ is the four velocity of the fluid (see, e.g., [12, 32, 33]). If we ignore hydrodynamics, this approach gives a friction force of the form $F_{\mathrm{fr}} = \eta v_w$ in the NR limit, where the coefficient η is a free parameter coming from the phenomenological damping term. Hence, setting η to the value η_{NR} from the microphysics calculation gives the correct friction force in this limit. This phenomenological model extrapolates the NR behavior ηv_w to a force of the form $\eta \gamma v$ for relativistic velocities, where v is the velocity of the fluid relative to the wall (which will vary across the wall, see below). However, this simple model does not give the friction saturation in the UR limit. In order to reproduce the saturating behavior, in ref. [34] a phenomenological model which gives a friction force of the form ηv was considered. However, such a model with a single free parameter η can hardly match both the NR and UR forces $\eta_{\mathrm{NR}} v$ and η_{UR}. In ref. [29] a phenomenological interpolation between the two regimes was considered.

For the subsonic velocities we are interested in, the exact dependence of the friction on the velocity does not introduce significant effects [29]. Therefore, we shall use the phenomenological scaling $\eta v \gamma$, which will allow us to use the results of the stability analysis [18]. We shall discuss the implications of this choice in section 4. In order to estimate the wall velocity for specific models, in section 3 we shall set the parameter η to the value η_{NR} coming from microphysics calculations.

Using this phenomenological approach to the friction, it is not difficult to include the hydrodynamics, i.e., to take into account the change of fluid variables across the wall. The fluid variables in each phase are related by matching conditions at the phase discontinuity. In the rest frame of the wall, we have [7]

$$
\begin{aligned}
w_u \gamma_u^2 v_u &= w_b \gamma_b^2 v_b, \\
w_u \gamma_u^2 v_u^2 + p_u &= w_b \gamma_b^2 v_b^2 + p_b, \\
\mathbf{v}_u^\perp &= \mathbf{v}_b^\perp,
\end{aligned}
\tag{2.4}
$$

where v is the component of the fluid velocity along the wall motion, $\mathbf{v}^\perp$ is the velocity in the transverse direction, and $\gamma = 1/\sqrt{1 - \mathbf{v}^2}$. By symmetry, we set $\mathbf{v}^\perp = \mathbf{0}$ for the stationary motion, but this component must be taken into account in the stability analysis. Furthermore, we define the incoming and outgoing flow velocities by $-v_u$ and $-v_b$, respectively, so that we deal with positive values of the variables v_u, v_b. Using suitable approximations (see appendix A), one obtains a friction force

$$F_{\mathrm{fr}} = \eta \left\langle \gamma v \right\rangle, \tag{2.5}$$

where $\langle f \rangle = \frac{1}{2}(f_b + f_u)$ for a quantity f defined on each side of the wall.

The thermodynamical quantities $w(T), p(T)$ in eqs. (2.4) are related by the equation of state. The treatment of hydrodynamics is considerably simplified by considering a simple approximation for the equation of state. This is particularly important for the stability analysis. In order to use the analytical results of ref. [18], we shall consider the bag EOS. This is the simplest EOS which can describe a phase transition.[3] Due to the difficulty of the stability analysis, it is not trivial to generalize the results of ref. [18] beyond these approximations. With these approximations, the driving force becomes

$$F_{\mathrm{dr}} = \frac{L}{4} \left(1 - \frac{T_u^2 T_b^2}{T_c^4} \right). \tag{2.6}$$

Several of the quantities in eqs. (2.5)–(2.6) are related through eqs. (2.4) and boundary conditions (see appendix A). As a result, the wall velocity v_w depends only on the temperature T_u, the coefficient η, and the parameter

$$\bar{L} \equiv L/w_u(T_c). \tag{2.7}$$

Notice that in general the driving force does not coincide with the pressure difference $p_b - p_u$, as one might expect, since it is nontrivially affected by hydrodynamics. Nevertheless, the fact that the pressure difference changes sign at $T = T_c$ is reflected in F_{dr}, which is very sensitive to the departure from the critical temperature. In particular, the reheating of the fluid causes a decrease of F_{dr}, acting as an effective friction [33, 36].

There are in general several solutions for v_w. The only solution for which the wall velocity is subsonic is the weak deflagration, and we shall only be interested in this case. Thus, in the bag approximation, we have $v_w < 1/\sqrt{3}$. The deflagration solution exists for large enough friction and small enough supercooling. For a deflagration, the fluid is reheated in front of the wall. Therefore, the temperature T_u is higher than the nucleation temperature T_n. The relation between T_u and T_n introduces an equation to solve together with that corresponding to the equilibrium of the forces (2.5)–(2.6). We write down all these equations in appendix A.

2.3 Stability of the deflagration

The possible hydrodynamic instabilities of cosmological phase-transition fronts have been investigated in refs. [15–18, 37–39]. The linear stability analysis of the wall-fluid configuration consists of considering small perturbations of the fluid variables on both sides of the wall, together with small deformations of the planar and infinitely thin wall. Below we briefly

---

[3]One limitation of this model is the fact that it gives a constant speed of sound $c_s = 1/\sqrt{3}$ in both phases, while the actual value of c_s may depart from this value [35].

sketch the generalities of the calculation for the deflagration case. For detailed and more general analysis, see [18, 39].

There are in principle seven variables, namely, the wall deformation ζ, the pressure fluctuations $\delta p_u, \delta p_b$, the variations of the fluid velocity along the propagation direction $\delta v_u, \delta v_b$, and the transverse velocities $v_u^\perp, v_b^\perp$. These perturbations depend on space and time. The three fluid fluctuations on a given side of the wall are related by the fluid equations. Linearizing these equations and looking for solutions of the form $\exp(i\mathbf{k} \cdot \mathbf{x}^\perp + qz + \Omega t)$, one obtains dispersion relations for $q(\mathbf{k}, \Omega)$, as well as algebraic equations relating the amplitudes of the different fluctuations. For the stability analysis one is interested in the unstable modes, which correspond to $\Omega > 0$ and $qz < 0$ [7]. For weak deflagrations, we have one unstable mode in front of the wall and two unstable modes behind it. We are thus left with four unknowns, namely, the amplitudes of the three unstable fluid modes and that of the wall perturbation. Finally, the fluid perturbations on the two sides of the wall are related by junction conditions at the wall, which are the counterparts of eqs. (2.4). There is also an equation for the perturbations of the surface, which is the counterpart of the equation $F_{\mathrm{dr}} = F_{\mathrm{fr}}$. As a consequence, one obtains a system of four algebraic equations for the four unknowns. The weak deflagration is linearly unstable if a nontrivial solution exists for this system.

Looking for linear instability is thus equivalent to demanding a 4×4 determinant to vanish. This gives an equation for the growth rate Ω as a function of the perturbation wavenumber $k \equiv |\mathbf{k}|$. For a complete treatment and analytic expressions we refer the reader to ref. [18]. The general result is that the deflagration is unstable for wavenumbers below a certain value k_c which depends on the thermodynamic parameters and the wall velocity. Nevertheless, depending on the parameters the critical wavenumber k_c may become negative, in which case all wavenumbers are stable. Demanding this to be the case (i.e., $k_c \leq 0$) one obtains a condition for the wall velocity, namely, $v_w \geq v_{\mathrm{crit}}$ for stability of the deflagration. The critical velocity v_{crit} corresponds to $k_c = 0$, which is equivalent to the equation[4]

$$\Delta v \left[\gamma_{sb}^2 \gamma_b (1 - \beta_b) - \frac{\gamma_b}{2} \right] + \frac{v_u}{\gamma_b^2} \left\langle \gamma_s^2 \gamma (1 - \beta) \right\rangle = 0, \tag{2.8}$$

where $\gamma_s^2 = 1 - v^2/c_s^2$, $\Delta v = v_b - v_u$. For the bag model, the quantity β is given by

$$\beta_{u,b} = \frac{4 \langle \gamma v \rangle v_{u,b}}{\gamma_{u,b} \left(\frac{T_c^4}{T_u^2 T_b^2} - 1 \right)}. \tag{2.9}$$

For $v_w < v_{\mathrm{crit}}$, perturbations with wavenumbers $0 < k < k_c$ grow exponentially. As discussed in section 4 below, for the electroweak phase transition the characteristic time for the development of the instabilities is generally much shorter than the time scales associated to bubble growth, even if v_w is very close to v_{crit}.

It is worth remarking that the critical value of the wall velocity does not depend on the friction coefficient η. The parameter η determines the *actual* value of v_w. The critical velocity v_{crit} can thus be associated to a critical friction η_{crit} (which could then be compared with the actual value of η in order to determine the stability). However, *the form* of the friction force (2.5) is implicit in the equations above. This is because, in the stability analysis, the coefficient η is eliminated by writing it as a function of the velocity and the driving force [16, 18].

---

[4]There are some sign differences with respect to ref. [18] because we have defined $v \equiv |v|$ for the fluid velocity in the wall frame.
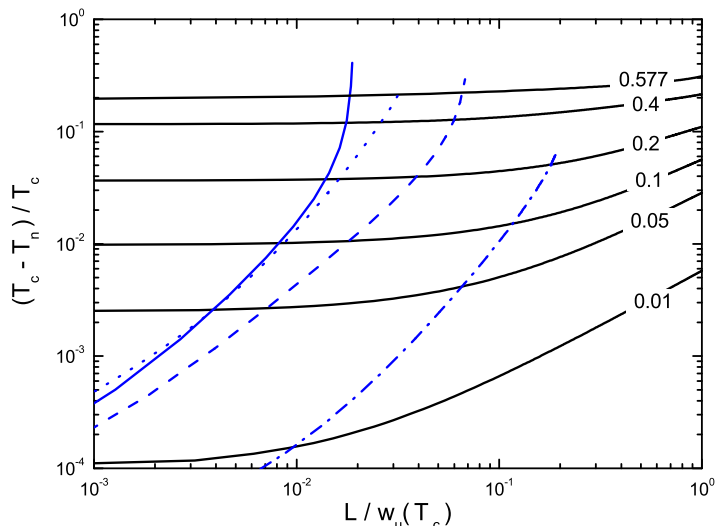
Figure 1. Curves of constant v_{crit} (solid black lines) in the plane of the parameters $\bar{L}$ and $1 - T_n/T_c$. Blue curves correspond to extensions of the SM considered below. Solid line: strongly coupled bosons (2 d.o.f.). Dashed line: strongly coupled bosons (12 d.o.f.). Dash-dotted line: strongly coupled fermions. Dotted line: dimension-six operator.

The critical velocity depends only on the dimensionless parameters $\bar{L}$ and T_n/T_c. Both parameters range between 0 and 1 and quantify the amounts of latent heat and supercooling, respectively. In figure 1 we show the curves of constant v_{crit} in the space of these two parameters [we considered the parameter $(T_c - T_n)/T_c$ since in many physical cases the temperature is very close to T_c]. These curves are model independent. We also show the points in this plane corresponding to some of the specific models considered below (those which span larger regions of the plane). The limit $\bar{L} \to 0$, $T_c - T_n \to 0$ corresponds to a second-order phase transition. The critical velocity increases with the amount of supercooling but is rather insensitive to the latent heat. The curves of constant v_{crit} accumulate at the weak deflagration limit $v_{\text{crit}} = c_s \simeq 0.577$. For values of the parameters above this curve, there is no critical velocity and any subsonic velocity is unstable. In appendix B we consider in more detail the dependence of v_{crit} on these parameters and we give a simple fit for $v_{\text{crit}}(\bar{L}, T_n/T_c)$.

In figure 1 it seems that, for physical models, none of the two parameters $\bar{L}$ or $(T_c - T_n)/T_c$ can reach the upper value 1. In fact, the supercooling parameter may in principle take values arbitrarily close to 1, since the nucleation temperature T_n can be very small for models with barriers in the zero-temperature effective potential. The upper limits of $(T_c - T_n)/T_c$ in these curves are due to the break-down of our calculations for such strong phase transitions. On the other hand, it is true that the latent heat tends to take relatively small values $\bar{L} \lesssim 0.1$ for physical models, as seen in the figure. This is because, in general, the entropy released in the phase transition is only a fraction of the total entropy. This fraction is proportional to the fraction of degrees of freedom (d.o.f.) which are strongly coupled to the Higgs.

As can be seen in figure 1, the wide range of possible amounts of supercooling implies a wide range of possible values of the critical velocity v_{crit}. On the other hand, the actual value of the wall velocity, v_w, also grows with the amount of supercooling, and it is not easy to guess, without specific calculations, in which cases the deflagration will be unstable. We perform such calculations in the next section.

3 Electroweak phase transition models

Several extensions of the SM have been considered in the literature in order to increase the strength of the phase transition and obtain a sizeable electroweak baryogenesis. Constraints from the recent LHC results threaten the viability of baryogenesis in some models (see, e.g., [40–42]). Since our aim is a general investigation of the possible instability, we shall not discuss the implications of experimental constraints. Our results will give in principle an additional constraint for the baryogenesis scenario. Furthermore, we shall not limit ourselves to the case of strongly first-order phase transitions, since the instability of the stationary wall propagation may have cosmological consequences even for weakly first-order phase transitions.

A classification of models for the electroweak phase transition was recently given in ref. [40]. Besides these model classes, we shall consider a model with TeV fermions introduced in ref. [43] as well as two-loop effects. For simplicity, we shall consider a single background field ϕ. For several extensions of the SM, ϕ corresponds to the SM Higgs, $\langle H^0 \rangle \equiv \phi/\sqrt{2}$. In extensions in which more than one scalar develop a vacuum expectation value (VEV), it is sometimes a good approximation to consider a single field ϕ, corresponding to a certain trajectory in field space.

3.1 Free energy and friction

We shall consider the one-loop finite-temperature effective potential given by

$$\mathcal{F}(\phi, T) = V_0(\phi) + V_1(\phi) + \mathcal{F}_1(\phi, T), \tag{3.1}$$

where V_0 is the tree-level potential and V_1, $\mathcal{F}_1$ are the zero-temperature and finite-temperature parts of the one-loop correction. These corrections receive contributions from the SM particles and from beyond-SM particles. We shall consider a spontaneous symmetry-breaking potential of the form

$$V_0(\phi) = -m^2 \phi^2 + \frac{\lambda}{4}\phi^4 + \frac{\lambda}{4}v^4 \tag{3.2}$$

as well as some tree-level modifications. Here, the parameters m and λ are related to the Higgs mass and VEV by $v = \sqrt{2/\lambda}\, m = 246\,\text{GeV}$, $m_H = \sqrt{2\lambda v^2} = 125\,\text{GeV}$, and the constant term in eq. (3.2) was added so that the potential vanishes at the minimum, i.e., $V(v) = 0$. We shall assume Higgs-dependent masses of the form

$$m_i^2(\phi) = h_i^2 \phi^2 + \mu_i^2, \tag{3.3}$$

and we shall consider the renormalized one-loop zero-temperature correction

$$V_1(\phi) = \sum_i \frac{\pm g_i}{64\pi^2} \left[m_i^4(\phi) \left(\log \frac{m_i^2(\phi)}{m_i^2(v)} - \frac{3}{2} \right) + 2m_i^2(\phi)m_i^2(v) - \frac{m_i^4(v)}{2} \right], \tag{3.4}$$

where the upper and lower signs correspond to bosons and fermions, respectively, and g_i is the number of d.o.f. of particle species i. This expression corresponds to the renormalization conditions that the tree-level values of the minimum and Higgs mass are not shifted by radiative corrections, i.e., $V_1'(v) = 0$, $V_1''(v) = 0$ (where a prime indicates a derivative with respect to ϕ). We have added a term $m_i^4(v)/2$ to the well known expression, so that the true vacuum energy density is not shifted either, i.e., $V_1(v) = 0$. Thus, in the symmetric phase we will have a false vacuum energy density given by $\rho_{\text{vac}} = V_0(0) + V_1(0)$, which contributes

to the Hubble rate during the phase transition. Finally, the one-loop finite-temperature correction, including the resummed daisy diagrams, is given by [44]

$$\mathcal{F}_1(\phi, T) = \sum_i \pm \frac{g_i T^4}{2\pi^2} \int_0^\infty dx\, x^2 \log\left[1 \mp \exp\left(-\sqrt{x^2 + m_i^2(\phi)/T^2}\right)\right]$$
$$+ \sum_{\text{bosons}} \frac{g_i T}{12\pi} \left[m_i^3(\phi) - \mathcal{M}_i^3(\phi)\right]. \tag{3.5}$$

The last term in eq. (3.5) receives contributions from all the bosonic species. We have $\mathcal{M}_i^2(\phi) = m_i^2(\phi) + \Pi_i(T)$, where $\Pi_i(T)$ are the thermal masses. For the transverse polarizations of the gauge bosons we have $\Pi(T) = 0$ and the last term in (3.5) vanishes.

In general, eqs. (3.1)–(3.5) give a phase transition at a certain temperature T_c from the high-temperature symmetric phase to the low-temperature broken-symmetry phase. The dynamics of the phase transition depends mostly on the difference

$$V_T(\phi) \equiv \mathcal{F}(\phi, T) - \mathcal{F}(0, T). \tag{3.6}$$

Depending on the particle content of the model, the phase transition may be first order, i.e., the effective potential may have two minima separated by a barrier. This is better appreciated in the high-temperature approximation, i.e., when eq. (3.5) admits an expansion in a power series of m/T. For masses of the form (3.3) we obtain the well known simple form [45]

$$V_T(\phi) = D\left(T^2 - T_0^2\right)\phi^2 - ET\phi^3 + \frac{\lambda_T}{4}\phi^4, \tag{3.7}$$

with coefficients given approximately by

$$D = \sum_i \tilde{c}_i \frac{g_i h_i^2}{24}, \quad T_0^2 = \frac{1}{D}\frac{m_h^2}{4}, \quad E = \sum_{\text{t.g.b.}} \frac{g_i h_i^3}{12\pi}, \quad \lambda_T = \lambda, \tag{3.8}$$

with $\tilde{c}_i = 1$ for bosons and $1/2$ for fermions.[5] We have neglected for simplicity corrections to these coefficients which are suppressed by factors of order $g_i/(32\pi^2)$. The terms $m^4 \log m^2$ in (3.4) cancel out with similar terms in the expansion of the thermal integrals in eq. (3.5), and only a dependence of the form $\phi^4 \log T^2$ remains. This gives a soft dependence of the coefficient λ_T on T, which was neglected in the approximation (3.8). For the coefficient E the sum runs only over transverse gauge bosons. Indeed, only the bosonic thermal integral has a cubic term $\sim (m/T)^3$ in its power expansion. The last term in eq. (3.5) replaces m^3 with $\mathcal{M}^3$ and we actually have

$$-\frac{gT}{12\pi}\left[h^2\phi^2 + \mu^2 + \Pi(T)\right]^{3/2}. \tag{3.9}$$

For gauge bosons we have $\mu = 0$, and for their transverse polarizations we also have $\Pi = 0$. Hence, only in this case we obtain a contribution to the term $-ET\phi^3$.

It is well known that, for an effective potential of the form (3.7), it is precisely the cubic term the one which allows a first-order phase transition, while for $E = 0$ the transition is second order. Indeed, the value of the order parameter at the critical temperature is given

---

[5]Besides, we have $\mathcal{F}(0, T) \simeq \rho_{\text{vac}} - \frac{\pi^2}{90}g_* T^4$, where $g_* = \sum_i c_i g_i$, with $c_i = 1$ for bosons and $7/8$ for fermions. For the SM, we have $g_* \simeq 107$.

by $\phi_b(T_c)/T_c = 2E/\lambda_{T_c}$. For the minimal SM, the constant E is very small and eq. (3.7) gives a very weakly first-order phase transition.[6] The relevant SM contributions to the one-loop effective potential come from the Z and W bosons, the top quark, and the Higgs and Goldstone bosons. The Higgs sector is usually ignored in the one-loop radiative corrections. This should be a good approximation in extensions of the SM which include particles with strong couplings to ϕ. We shall use this simplification. Therefore, the ϕ-dependent masses are of the form $h_i\phi$, with $h_i = m_i/v$, where m_i are the physical masses at zero temperature. Thus, in the case of the SM we have

$$D_{\mathrm{SM}} = \left(2h_W^2 + h_Z^2 + 2h_t^2\right)/8, \ E_{\mathrm{SM}} = \left(2h_W^3 + h_Z^3\right)/6\pi. \tag{3.10}$$

Since only bosons contribute to the parameter E, extensions of the SM containing extra bosons are often considered in the literature. However, a cubic term in the effective potential is difficult to obtain due to the thermal mass $\Pi \sim h^2T^2$ in eq. (3.9). This has lead to the investigation of scenarios in which a negative squared mass cancels the thermal mass, $\mu^2 \simeq -\Pi(T)$. For high values of the couplings h_i the expansion (3.7) breaks down. In this case, the one-loop terms $\phi^4 \log \phi$ in the zero-temperature effective potential (3.4) may strengthen the phase transition by causing a barrier at $T = 0$. Two loop contributions and tree-level modifications to the effective potential have also been considered in order to increase the strength of the electroweak phase transition. In the present paper we shall consider all these extensions of the SM.

A simple approximation for the general dependence of the friction coefficient η on the parameters of the model was derived in refs. [46, 47]. We shall use this approximation to estimate the wall velocity (for a different approach see [48]). In this approximation, η receives contributions from particles which obey the Boltzmann equation as well as from infrared excitations of bosonic fields, which are treated classically. The contribution of Boltzmann particles is given by

$$\eta_B = \sum_i \frac{g_i h_i^4}{\bar{\Gamma}/T} T \int_0^{\phi_c} \left[c_1(m_i/T)\right]^2 (\phi/T)^2 \sqrt{2V_T}\, d\phi, \tag{3.11}$$

where $\phi_c = \phi_b(T_c)$, the function c_1 is given by

$$c_1(x) = \frac{1}{2\pi^2} \int_x^\infty dy\, \sqrt{y^2 - x^2} \frac{e^y}{(e^y \mp 1)^2}, \tag{3.12}$$

and $\bar{\Gamma}$ is an average interaction rate arising from the collision terms of the Boltzmann equations. The friction decreases with this parameter since the deviations from the equilibrium distributions in front of the wall will be smaller if the processes are quicker. For the electroweak phase transition, $\bar{\Gamma}$ is typically $\sim 10^{-2}T$. The infrared bosons contribution is given by

$$\eta_{\mathrm{ir}} = \sum_{\mathrm{bosons}} \frac{g_i h_i^4 \pi m_D^2}{8T^2} T \int_{\phi_0}^{\phi_c} b(m_i/T) (\phi/T)^2 \sqrt{2V_T}\, d\phi, \tag{3.13}$$

where m_D is the Debye mass, given by $m_D^2 = (11/6)g^2T^2$ for the W and Z bosons of the SM, and $m_D^2 = h^2T^2/3$ for a scalar singlet. The integral in (3.13) has an infrared cut-off ϕ_0 for

---

[6]Moreover, the small value of ϕ_b/T causes perturbation theory to break down and only non-perturbative calculations become reliable.

small μ_i, given by $\phi_0 = \sqrt{L_w^{-2} - \mu_i^2}/h_i$ for $\mu_i < L_w^{-1}$, and $\phi_0 = 0$ for $\mu_i > L_w^{-1}$, where L_w is the wall width. In the thin wall approximation, L_w can be estimated as $L_w \approx \int_{0.1\phi_c}^{0.9\phi_c} d\phi/\sqrt{2V_T}$. The function b is given by

$$b(x) = \frac{1}{2\pi^2} \int_x^\infty \frac{dy}{y^3} \frac{e^y}{(e^y - 1)^2}. \tag{3.14}$$

The two contributions dominate in different parameter regions, and we have $\eta = \eta_B + \eta_{\rm ir}$.

Depending on the model, we shall use either the full one-loop effective potential (3.4)–(3.5) or its high-temperature expansion (3.7). In the former case, we shall use the friction coefficients (3.11) and (3.13), while in the latter case we shall use a similar high-temperature approximation for the friction coefficients,

$$\eta_B = \sum \frac{g_i h_i^4}{\bar{\Gamma}/T} \left(\frac{\log \chi_i}{2\pi^2} \right)^2 \frac{\phi^2 \sigma}{T}, \tag{3.15}$$

$$\eta_{\rm ir} = \sum_{\rm bosons} \frac{g_i m_D^2 T}{32\pi L_w} \log \left(m_i(\phi) L_w \right), \tag{3.16}$$

and $L_w \approx \phi^2/\sigma$. Here, $\chi_i = 2$ for fermions and $\chi_i = m_i(\phi)/T$ for bosons, and σ is the surface tension of the bubble wall.

3.2 The SM with a low Higgs mass

For comparison with previous results, we consider first the unrealistic case of the SM with a light Higgs. We also consider larger Higgs masses (although for large m_H the perturbative expansion breaks down) in order to analyze the dependence of the velocity on the strength of the phase transition. For this model we use the approximation (3.7) for the effective potential as well as the approximations (3.15)–(3.16) for the friction. The result is shown in figure 2.

The critical velocity for this model (solid line) agrees in order of magnitude, but not exactly, with ref. [16]. For instance, for $m_H = 60\,{\rm GeV}$, they obtain $v_{\rm crit} \simeq 0.035$, while we obtain $v_{\rm crit} \simeq 0.022$. As already mentioned, as a function of the thermodynamic parameters, our result for $v_{\rm crit}$ is in good agreement with ref. [16]. The present discrepancy is due to the rough estimation of the temperature T_u for this model in ref. [16].

The dotted line in figure 2 corresponds to the wall velocity obtained from the calculation of the friction using only the Boltzmann equations. We remark that our approximation contains a single, effective rate $\bar{\Gamma}$ instead of the several collision-term parameters coming from the different interactions. Setting $\bar{\Gamma} = 10^{-2}T$, the values of v_w, as well as the dependence on m_H, agree with the results of ref. [21] (and are also close to those of [31]). We stress that the calculations of refs. [21, 31] omit the contribution of infrared boson excitations to the friction, which can make the wall velocity significantly smaller [23]. In the case of the SM, the infrared term receives contributions from the gauge bosons. The result for the complete friction is shown in a dashed line in figure 2. This result agrees with the estimations of ref. [23].

We see that the infrared contribution to the friction dominates for weakly first-order phase transitions, and causes the deflagration to become unstable (i.e., $v_w < v_{\rm crit}$).

3.3 Negative squared mass (thermal cubic term)

The simplest extension of the SM consists of adding one or more gauge-singlet scalars S_i (see, e.g., [49, 50]). In many models, these bosons constitute a hidden sector which couples only to the SM Higgs doublet through the so called Higgs portal operator $h_s^2 H^\dagger H \sum S_i^2$
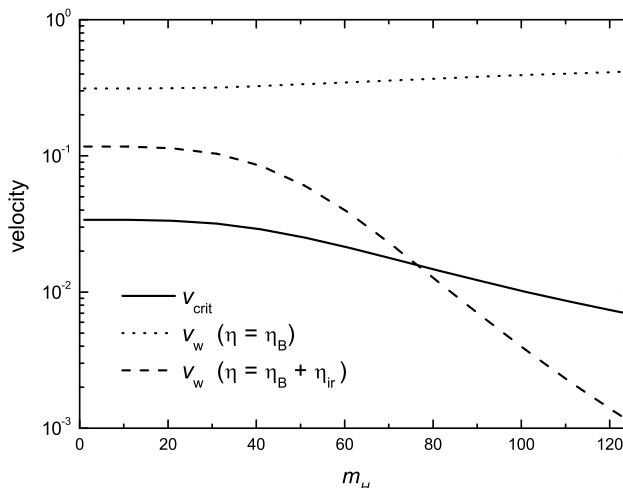
Figure 2. The critical velocity v_{crit} and the wall velocity v_w for the SM with a low Higgs mass.

(assuming, for simplicity, real fields and universal couplings $h_i = h_s$). The scalars may have SU(2) × U(1)-invariant mass terms $\mu_s^2 S^2$ as well as quartic terms $\lambda_s S^4$. For the moment we shall not consider the possibility that S develops a VEV.

If $h_s \phi_b(T)/T$ is not too large, the free energy is of the form (3.7), with the cubic term replaced by the term (3.9). The latter is not as effective as a cubic term in strengthening the phase transition. The thermal mass is given by $\Pi = (h_s^2 + \lambda_s)T^2/3$ [50]. A negative value of μ_s^2 may enhance the strength of the phase transition, since for $\mu_s^2 \simeq -\Pi(T)$ the term (3.9) is effectively of the form $-T\phi^3$. This fact is exploited in the case of the MSSM in the light-stop scenario [51]. Notice that negative values of μ_s^2 may induce a nonvanishing expectation value of the extra scalar. For the case of top squarks, this introduces the danger of color breaking minima. We shall not take into account this issue here. For the moment we will just consider the SM plus g_s extra bosonic degrees of freedom. We thus have an effective potential of the form

$$V_T(\phi) = D\left(T^2 - T_0^2\right)\phi^2 - TE\phi^3 - \frac{g_s T}{12\pi}\left[h_s^2\phi^2 + \frac{h_s^2 + \lambda_s}{3}T^2 + \mu_s^2\right]^{3/2} + \frac{\lambda}{4}\phi^4, \qquad (3.17)$$

with $D = D_{\text{SM}} + g_s h_s^2/24$, $E = E_{\text{SM}}$, $T_0^2 = (m_h^2/4)/D$, and $\lambda = m_H^2/(2v^2)$.

For definiteness, we consider the case $g_s = 6$ and $\lambda_s = 0.5$ (below we consider a different value of λ_s). In figure 3 we show the wall velocity and the critical velocity for a couple of values of the coupling h_s, namely, $h_s = 0.7$ (left panel) and $h_s = 0.8$ (right panel). We let μ_s^2 vary in the range $[-\Pi(T_0), \Pi(T_0)]$ (we have $T_c \simeq T_0$). The dotted curves indicate the value of the order parameter $\phi_b(T)/T$ at $T = T_c$ (lower curve) and at $T = T_n$ (upper curve). Since the plasma is reheated during the expansion and collisions of bubbles, it is not clear which one is the appropriate value for the baryogenesis condition (1.1). The conservative bound is $\phi_b(T_c)/T_c$. Only for μ_s^2 close to $-\Pi(T)$ the contribution of the boson gives a cubic term. Thus, the strength of the phase transition reaches a maximum at this end. Nevertheless, the strength of the phase transition is also enhanced as g_s or h_s are increased. For $h_s = 0.7$ the value $\phi_b/T = 1$ is not reached even in the limit $\mu_s^2 \simeq -\Pi(T)$, while for $h_s = 0.8$ we have $\phi_b/T \gtrsim 1$ for $\mu^2 < 0$.
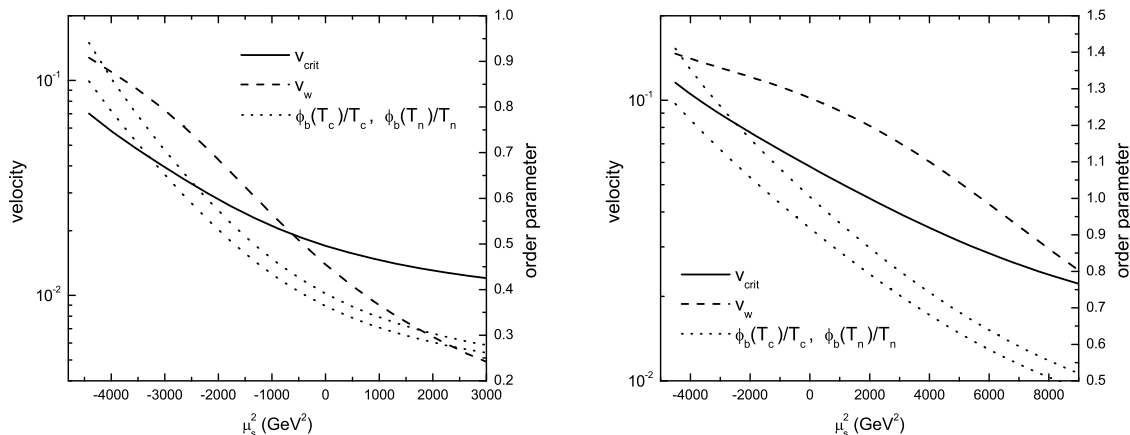
Figure 3. The critical velocity v_{crit}, the wall velocity v_w, and the order parameter for an extension of the SM with 6 singlet scalars, for $\lambda_s = 0.5$ and $h_s = 0.7$ (left panel) and $h_s = 0.8$ (right panel).

We have checked that for different values of g_s or h_s the behavior of the various curves is qualitatively similar. For weakly first-order phase transitions with small values of ϕ_b/T we have a small v_w as well as a small v_{crit}, while for more strongly first-order transitions both v_w and v_{crit} are higher. On the other hand, their values generally cross at a certain point (as can be appreciated in the left panel of figure 3). Thus, we have $v_w < v_{\text{crit}}$ for weak enough phase transitions ($\phi_b/T < 0.5$) and $v_w > v_{\text{crit}}$ for stronger phase transitions. In particular, for $\phi_b/T \geq 1$ we obtain stable deflagrations. Notice, however, that the curves of v_w and v_{crit} begin to approach each other again as the strength of the phase transition continues increasing. As we shall see below, for very strong phase transitions we will have $v_w < v_{\text{crit}}$ again.

For $g_s = 6$ and $h_s \simeq 0.7$ this model can be regarded as a toy model for the light stop scenario of the MSSM, consisting of the SM plus the light right-handed top squark (stop). At the one-loop order and disregarding the possibility that the extra scalar develops a VEV, the main quantitative difference with the realistic case appears in the resummed daisy diagrams. The main contribution to the thermal mass of the stop is of the form $4g_{\text{str}}^2 T^2/9$, where g_{str} is the strong gauge coupling [51]. In our numerical calculation, we obtain the same effect by setting the parameter λ_s in eq. (3.17) to the value $4g_{\text{str}}^2/3$. This increases considerably the value of $\Pi(T)$ and, hence, the value of the negative squared mass needed to compensate this thermal mass. The collision terms in the Boltzmann equations are also different due to a different particle content. This effect may be relevant if the wall velocity is close to the critical value. For the MSSM we can choose the value of our effective rate $\bar{\Gamma}$ in order to match the result of the detailed microphysics calculation [22]. Turning off the infrared contribution to the friction and setting[7] $m_H = 110\,\text{GeV}$ as in [22], the wall velocity should vary around $v_w = 0.1$ (the friction is higher than in the SM due to the coupling of the extra boson with the Higgs). We obtain the correct v_w for $\bar{\Gamma} = 5 \times 10^{-3}T$.

The lower, blue curves of figure 4 show the estimated wall velocity (including the infrared part of the friction) together with the critical value for this case. The result is plotted as a function of μ_s^2 as well as of the mass of the extra scalar, which is given by $m_s = \sqrt{h_s^2 v^2 + \mu_s^2}$. We considered values of μ_s^2 from $-\Pi(T_0)$. For this value of μ_s^2, the infrared contribution to

---

[7]In fact, the value of m_H does not affect significantly the Boltzmann result, as observed in the dotted curve of figure 2.
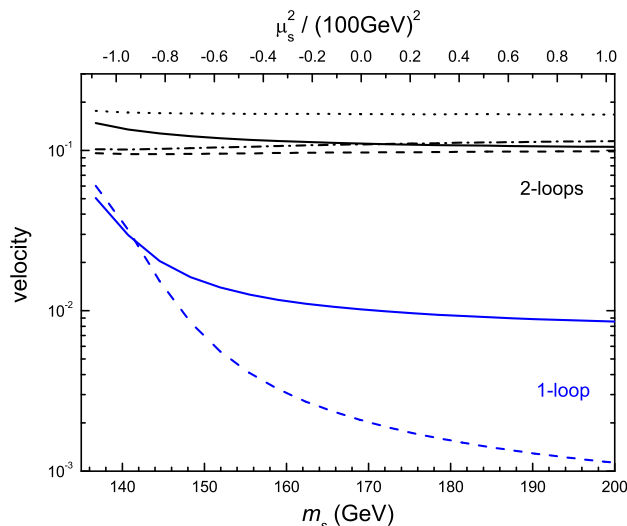
Figure 4. The critical velocity (solid lines) and the wall velocity (dashed lines) for the case of the SM plus a light stop. The two lower (blue) lines correspond to considering only the 1-loop potential. The upper (black) lines correspond to including the 2-loop correction. The dash-dotted line corresponds to turning off the contribution of infrared fields. The dotted line corresponds to increasing the value of the parameter $\bar{\Gamma}$ by a factor of 2.

the friction lowers the wall velocity from $v_w \simeq 0.1$ to $v_w \simeq 0.05$, and the effect is stronger for weaker phase transitions (dashed blue curve).

We see that we have $v_w < v_{\rm crit}$, except for μ_s^2 very close to $-\Pi(T_0)$. In any case, we obtained values of $\phi_b(T_c)/T_c$ smaller than 0.7 even in this limit. Indeed, in this scenario a phase transition which is strong enough for baryogenesis is obtained only for unrealistic values of the Higgs mass. The situation improves when two-loop corrections are considered.

3.4 Two-loop effects (the MSSM)

Although the light stop scenario does not give a strong enough phase transition at one-loop order, two-loop corrections can make the phase transition strongly first-order even without requiring negative μ_s^2 [52, 53]. The most important two-loop corrections are of the form $\phi^2 \log \phi$,

$$V_2\left(\phi, T\right) \approx C \frac{T^2 \phi^2}{32\pi^2} \log\left(\frac{\phi}{T}\right). \tag{3.18}$$

We consider such a contribution by adding to the potential (3.17) a term of the form (3.18), with a coefficient $C = 6h_s^4 - 8g_{\rm strong}^2 h_s^2$ coming from the MSSM stop and gluon loops.

The results for the wall and critical velocities with this modification are shown in figure 4 (upper, black curves). We obtain a higher critical velocity $v_{\rm crit} \simeq 0.1$-0.15 (black solid line) as well as a higher wall velocity $v_w \simeq 0.1$ (black dashed line), but we have $v_w < v_{\rm crit}$. Notice that the strength of the phase transition is essentially due to the presence of the term (3.18) in the effective potential. As a consequence, the result has a very soft dependence on m_s. The significant increase of the wall velocity with respect to the one-loop value is due to the fact that the two-loop term does not change the particle content of the model (hence the friction cannot increase significantly) but does increase the strength of the phase transition. In this approximation we obtain $\phi_b/T \gtrsim 1$ for all the range of μ_s^2 considered.

Since the wall velocity is so close to the critical value, the uncertainties in the calculation of v_w become relevant. In this case the Boltzmann part of the friction dominates. This can be seen by turning off the infrared contribution, which results in the dash-dotted curve of figure 4. Since the friction is dominated by the Boltzmann term, the $\mathcal{O}(1)$ errors in the estimation of collision terms are consequential for the stability of the deflagration. To see the sensitivity to the parameter $\bar{\Gamma}$, let us consider again the SM-like value $\bar{\Gamma} = 10^{-2}T$ instead of the MSSM-like value $\bar{\Gamma} = 5 \times 10^{-3}T$. This gives the dotted curve,[8] which is safe from the instability. On the other hand, a different approximation for the friction [48] (which gives similar values for the one- and two-loop effective potentials) gives $v_w \sim 0.05$. Such deflagrations would be clearly unstable, since the velocity is a factor of 2 below the critical value.

Therefore, a more accurate determination of v_w would be important for this model. It is also important to remark that in baryogenesis calculations the wall velocity is often assumed to be $v_w \lesssim 0.1$, which is just below the lower bound v_{crit} for this model. Moreover, this model is severely constrained by experimental data (see, e.g., [54]). We stress that we have considered a simplified version of the light stop scenario, which has several parameters we just have not taken into account. In spite of this, we do not expect a significant difference for the critical velocity in the realistic case, although we do expect $\mathcal{O}(1)$ factors in the wall velocity, as already discussed.

3.5 Tree-level effects

Real gauge-singlets allow cubic terms of the form S^3 or $H^\dagger H S$. Such corrections to the Lagrangian arise in extensions of the SM with a singlet (see, e.g., [55–60]) as well as in extensions of the MSSM (see,e.g., [61–64]). The presence of cubic terms in the tree-level potential makes it easier to get a strongly first-order electroweak phase transition. Indeed, the strength of the transition is dominated by such cubic terms, which provide a barrier already at zero temperature. In order to study this effect, one should consider the effective potential for the condensates of the two fields H and S. However, our numerical computation of the nucleation temperature is based on a single-variable potential. In order to incorporate this kind of model into our generic analysis, we shall assume that the thermal tunneling occurs through a trajectory in configuration space which can be parameterized with a single field $\phi(x)$, and that along this trajectory the zero-temperature effective potential has a cubic term [40]. This is equivalent to considering a toy model which consists of adding a term $-A\phi^3$ to the tree-level potential (3.2), where A is a free parameter with mass dimensions [47]. In this model the parameters of the potential are related to the physical Higgs VEV and mass by $2m^2 = \lambda v^2 - 3Av$, $m_H^2 = 2\lambda v^2 - 3Av$.

We thus consider the high-temperature effective potential (3.17) plus a term $-A\phi^3$. We consider values of the parameters as in the left panel of figure 3 ($g_s = 6$, $h_s = 0.7$, $\lambda_s = 0.5$, $\bar{\Gamma}/T = 0.01$) with $\mu_s = 0$. We show the result in the left panel of figure 5. We have considered values of the parameter A for which $h_s\phi_b(T_n)/T_n \lesssim 1$, so that the high-temperature expansion is valid. The strength of the phase transition grows quickly with A, and values $\phi_b/T > 1$ are reached for values of A which are much smaller than the scale v. In this parameter range we obtain subsonic velocities. These deflagrations are stable on almost the entire considered range.

Another possible tree-level modification is the introduction of non-renormalizable operators. In particular, a dimension-six term of the form $(H^\dagger H - v^2/2)^3/\Lambda^2$ gives a negative

---

[8]In ref. [47] an even higher value $\bar{\Gamma} = 5 \times 10^{-2}$ was used for this model, obtaining as a consequence higher values of the wall velocity ($v_w \simeq 0.4$-0.45).
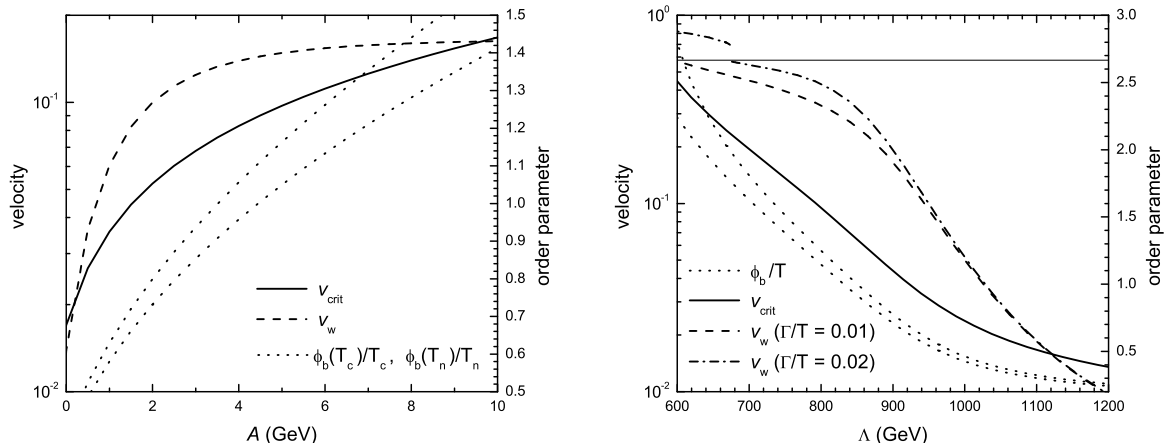
Figure 5. Left panel: the SM plus a singlet, with a cubic term in the scalar sector. Right panel: the SM plus a sextic operator. The horizontal line indicates the speed of sound.

quartic coupling if the cutoff is low enough [65–69]. We thus consider the SM plus a term of this form, which gives a term $\left(\phi^2 - v^2\right)^3/(8\Lambda^2)$ in the effective potential. Adding this term to the tree-level potential (3.2) does not shift the value of the minimum nor the Higgs mass, i.e., we have $v^2 = 2m^2/\lambda$, $m_H^2 = 2\lambda v^2$. The sextic operator introduces the terms

$$+ \frac{3v^4}{8\Lambda^2}\phi^2 - \frac{3v^2}{2\Lambda^2}\frac{\phi^4}{4}, \tag{3.19}$$

which modify the quadratic and quartic terms of the effective potential and, in particular, may change their sign. Thus, for $\Lambda < \sqrt{3/2}v^2/m_H \simeq 600\,\mathrm{GeV}$ the quadratic term becomes positive (already at zero temperature). Nevertheless, for $\Lambda < \sqrt{3}v^2/m_H \simeq 840\,\mathrm{GeV}$ the quartic term becomes negative, causing a barrier in the zero-temperature effective potential, which is stabilized by the term $+\phi^6/(8\Lambda^2)$. For this calculation we use the full one-loop correction (3.5) instead of its high-temperature approximation.

The results for this model are shown in the right panel of figure 5 as functions of the cutoff. Below $\Lambda \simeq 850\,\mathrm{GeV}$ we have $\phi_b(T)/T > 1$. Since the particle content is the same as in the SM, we set again $\bar{\Gamma} = 0.01$. The values of the wall velocity (dashed line) are in good agreement with those of ref. [31] for stronger phase transitions (for instance, for $\Lambda = 700\,\mathrm{GeV}$ we obtain $v_w = 0.45$ while in [31] the result is $v_w = 0.46$). For weaker phase transitions we obtain smaller values of v_w (e.g., $v_w \simeq 0.17$ for $\Lambda = 900\,\mathrm{GeV}$, in contrast to $v_w = 0.27$ in [31]). This is to be expected since, for weaker phase transitions, the infrared part of the friction becomes noticeable. Notice that v_w is subsonic in all the range of Λ we considered, but it approaches the speed of sound for $\Lambda \simeq 600\,\mathrm{GeV}$. Therefore, an $\mathcal{O}(1)$ variation of the friction coefficient may give supersonic solutions. To illustrate this we consider the value $\bar{\Gamma}/T = 0.02$ (dash-dotted line). In this case, detonation solutions appear below $\Lambda \simeq 675\,\mathrm{GeV}$. Notice also that the curves for the two values of $\bar{\Gamma}$ coincide for weaker phase transitions, where the infrared contribution dominates the friction.

Regarding the stability, we see that the wall velocity becomes smaller than the critical value (solid line) only for weak phase transitions with $\phi_b/T < 0.3$, corresponding to wall velocities $v_w \lesssim 0.015$.

– 17 –
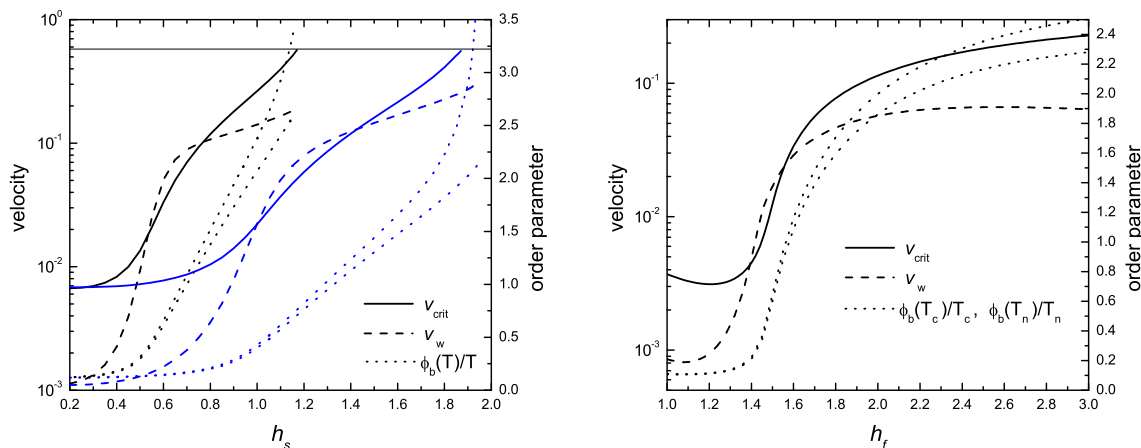
Figure 6. The critical velocity, the wall velocity, and the order parameter as functions of the coupling of the extra particles to the Higgs. Left panel: 12 real scalars (in black) and 2 real scalars (in blue). Right panel: 12 fermionic d.o.f.

3.6 Strong coupling

Let us consider again the extension of the SM with a singlet scalar. This time however, instead of considering a negative μ_s^2 in order to change the strength of the phase transition, we shall set $\mu_s = 0$ and vary the coupling to the Higgs. Therefore, the ϕ-dependent mass is given by $m_s^2(\phi) = h_s^2\phi^2$. Besides the cubic term, for high enough h_s, the zero-temperature term $m_s^4 \log m_s^2$ in eq. (3.4) becomes relevant. A barrier in the effective potential appears at zero temperature, and the size of this barrier grows as h_s is increased. This increases the strength of the phase transition and, as a consequence, the $\phi^4 \log \phi$ term becomes even more important. In this case we may have large values of the order parameter ϕ_b/T [47, 70, 71], and we shall not use the high-temperature expansion.

For simplicity, we consider $\lambda_s = 0$. The results are qualitatively similar in the general case (we have checked this) since λ_s only affects the value of the thermal mass. We show the values of the velocity and the order parameter in the left panel of figure 6 as functions of h_s for $g_s = 2$ bosonic degrees of freedom (lower, blue curves) and $g_s = 12$ (upper, black curves). The results are qualitatively very similar for the two cases, only that for smaller d.o.f. a higher coupling is needed to increase the strength of the transition. In both cases the deflagration is unstable for weak phase transitions ($\phi_b/T \lesssim 0.4$), there is a range of stable deflagrations, and for stronger phase transitions ($\phi_b/T \gtrsim 1.3$) the velocity is again smaller than $v_{\rm crit}$. This tendency is already seen in previous cases. There is also a range of values of h_s for which we have both $\phi_b/T > 1$ and stable deflagrations. In this range we have wall velocities $v_w \simeq 0.05$-0.1, which is good for baryogenesis. We obtained subsonic velocities, but varying the friction by an $\mathcal{O}(1)$ factor detonations may appear (see, e.g., ref. [72]).

Extra fermions strongly coupled to the Higgs field can also make the phase transition strongly first-order [43]. However, strongly coupled fermions may make the vacuum unstable due to the minus sign in front of the term $m_f^4 \log m_f^2$ in (3.4). This problem can be solved by adding heavy bosons with the same couplings but with a large ϕ-independent mass term, so that they are decoupled from the dynamics at $T \sim 100\,{\rm GeV}$. A particular model, considered in ref. [43], consists in a realization of split supersymmetry, where the standard relations between the Yukawa and gauge couplings are not fulfilled. In the simplest case, only $g_f =$

12 d.o.f. are coupled to the SM Higgs, with degenerate eigenvalues of the form $m_f^2(\phi) = \mu_f^2 + h_f^2\phi^2$. Here we consider for simplicity only the case $\mu_f = 0$. Perturbativity requires $h_f \lesssim 3.5$. The bosonic stabilizing fields have the same number of d.o.f., and a dispersion relation $m_b^2(\phi) = \mu_b^2 + h_b^2\phi^2$, with $h_b = h_f$ and

$$\mu_b^2 = \left[\exp\left(\frac{m_H^2 8\pi^2}{g_f h_f^4 v^2}\right) - 1\right] h_f^2 v^2, \tag{3.20}$$

which is the maximum value consistent with stability. For simplicity, $\Pi_b = 0$ is assumed.

In the right panel of figure 6 we show the results for this model as a function of the coupling h_f. The velocities, as well as the order parameter, are smaller than in the case of extra scalars. However, the behavior is qualitatively similar. In particular, there is a range of values of h_f for which the deflagration is stable (i.e., $v_w > v_{\text{crit}}$). In this range we have $v_w \sim 10^{-2}$. Values of the order parameter $\phi_b/T \simeq 1$ occur at the upper limit of this range and, thus, may be compatible with stability.

4 Consequences of the instability

So far we have only calculated the critical velocity below which the deflagration is unstable, and compared it with the actual value of the wall velocity. We now wish to discuss the possible consequences of the case $v_w < v_{\text{crit}}$.

Before doing so, it is worth discussing on the use of the phenomenological form $\eta v\gamma$ for the friction, explicit in the calculation of v_w and implicit in the calculation of v_{crit} (or, equivalently, of η_{crit}). Important deviations from this scaling may occur [31]. In particular, the friction should saturate in the ultra-relativistic regime [30], while this model grows unboundedly as $v_w \to 1$ due to the γ factor. We thus may expect significant errors for wall velocities close to the speed of sound or higher. Nevertheless, for small wall velocities (particularly those of interest for baryogenesis) our phenomenological model should give a good description. Indeed, notice that for the two models which admit a direct comparison with the results of [31] (namely, the SM with a low Higgs mass and the SM with a low cutoff, for which the particle content is that of the SM), our results for v_w (before taking into account the infrared part of the friction) are in good agreement with those of [31]. In any case, since the scaling $\eta v\gamma$ generally overestimates the friction force, we may expect both v_w and v_{crit} to be actually higher than our estimations. Therefore, since deflagrations with $v_w < v_{\text{crit}}$ are unstable, our estimation of v_{crit} gives a conservative lower bound for the velocity of a stable deflagration.

Let us now assume that we are in the case $v_w < v_{\text{crit}}$. Then, perturbations of the wall-fluid system in a range of wavenumbers $0 < k < k_c$ are unstable. In the first place, it is important to determine whether these instabilities will grow in a time comparable to the duration of the phase transition. There is a characteristic scale in the problem (see [18] for details), which is given by $d = \sigma/F_{\text{dr}}$, where σ is the surface tension and F_{dr} is the driving force. Thus, the deflagration wall is unstable for wavelengths λ which are higher than a critical value $\lambda_c \propto d$. The instabilities develop once the bubble reaches a size $R_b \sim \lambda_c$. The quantity d is generally of the order of the initial bubble size. In contrast, the final bubble size R_f is in general much higher than d. As a consequence, there will be instabilities in the range $\lambda_c < \lambda < R_f$.

To be more precise, in the limit of small supercooling, small latent heat, and small velocity we have $\lambda_c \sim d/[\bar{L}(1 - v_w/v_{\text{crit}})]$. Therefore, unless v_w is very close to v_{crit}, we have

$\lambda_c \sim d/\bar{L}$. Although $\bar{L}$ may be quite small and, hence, λ_c may be a few orders of magnitude larger than d, the final bubble size R_f will still be many orders of magnitude larger [18]. This is because R_f is related to the cosmological time H^{-1} (where H is the Hubble rate), while d is given by thermodynamical variables. Roughly, we have $R_f/d \sim M_P/T$, where M_P is the Planck mass. For the electroweak phase transition we have $M_P/T \sim 10^{17}$.

Hence, the instabilities generally begin to grow when bubbles are still very small. On the other hand, the instabilities need time to develop. The growth rate Ω in the linear regime is proportional to $\lambda - \lambda_c$ and to $1 - v_w/v_{\rm crit}$. A simple dynamical analysis shows that (in the approximation $T_n/T_c \simeq 1$, $\bar{L} \ll 1$, $v_w \ll 1$) the instabilities become important when the bubble size reaches the value $R_b^{\rm inst} \sim [\bar{L}\,(1 - v_w/v_{\rm crit})]^{-2}d$ [18]. Again, even though $\bar{L}$ may be quite small we will have $R_b^{\rm inst} \ll R_f$ unless v_w is extremely close to $v_{\rm crit}$. Therefore, the instabilities become important very early in the development of the phase transition.

As already discussed, the instability of the deflagration may spoil the mechanism of electroweak baryogenesis if the wall accelerates and reaches supersonic velocities. In fact, the linear stability analysis breaks down as the perturbations grow. Therefore, Ω only indicates the initial acceleration rate of the unstable wall. It is in principle possible that nonlinear effects stabilize the propagation of the phase transition front. In such a case, one may expect that the wall reaches a new stationary regime, perhaps with a higher velocity. Notice, however, that this new regime will not correspond to a stable weak deflagration, unless the conditions which determine v_w change. All other known stationary solutions (namely, Jouguet deflagrations and weak detonations) are supersonic.

There are (at least) two possible alternatives to this situation. Since the instabilities corrugate the wall, the growth of the bubble may be of dendritic type [73]. The hydrodynamics in this case may differ significantly from the case of planar (or spherical) walls, and there may be new stationary propagation modes. Another possibility is that, by the time the instabilities begin to become noticeable, the shock fronts coming from other bubbles already hit the wall. This may happen for small enough v_w, since the shock velocity is supersonic. In such a case, the plasma outside the bubble will be reheated from the initial temperature T_n to a higher temperature T_r. This reheating will tend to decrease both v_w and $v_{\rm crit}$, but the overall effect may be stabilizing. Indeed, the release of latent heat may reheat the plasma up to T_c. In such a case the phase transition necessarily slows down [74–76]. The effects of such a reheating on electroweak baryogenesis have been investigated in refs. [77–79].

Leaving aside these possibilities, the critical velocity sets a lower bound for the velocity of stationary phase transition fronts. This lower bound for the wall velocity may be used to constrain models of EWB in two ways. On the one hand, if the wall velocity for a given model is calculated and turns out to be below $v_{\rm crit}$, then in principle the wall will accelerate to velocities which are too high for EWB. This would rule out this model as a baryogenesis scenario. On the other hand, since an accurate calculation of v_w is too difficult and model-dependent, using the value of $v_{\rm crit}$ as a lower bound may be useful. This lower bound may constrain the baryogenesis mechanism if $v_{\rm crit}$ turns out to be too large.

Interestingly, besides the potentially negative consequences for baryogenesis, the instability of slow walls may give rise to new cosmological consequences for weak phase transitions. Indeed, the instabilities lead to acceleration of the walls, anisotropic growth of bubbles and turbulence of the plasma. These effects may give origin to magnetic fields [24] or gravitational waves [18].

5 Conclusions

It is known that the stationary motion of phase transition fronts may be unstable for subsonic velocities. Specifically, the deflagration front is hydrodynamically unstable below a critical velocity v_{crit}. In order to discuss the implications of this fact for the electroweak phase transition, we have computed both the wall velocity and the critical velocity for several extensions of the Standard Model. We have considered a significant variety of models and a wide range of parameters, including those which are favorable for baryogenesis.

The general result is that the deflagration tends to be unstable for very weak or very strong phase transitions, while for phase transitions with an order parameter $\phi_b/T \approx 1$ the deflagrations are generally stable. In general, for any model there is a range of parameters for which we have stable deflagrations.

The stability condition $v_w > v_{\text{crit}}$ constitutes in principle a restriction for electroweak baryogenesis (assuming that, if it is not fulfilled, the wall will accelerate to supersonic velocities). This condition, combined with that of avoiding the washout of the generated BAU (i.e., $\phi_b/T \gtrsim 1$), the requirement of enough CP violation, and experimental bounds, may restrict significantly some models. We remark that, even if we have a subsonic wall with $v_w > v_{\text{crit}}$, a departure of the wall velocity from the range $10^{-2} < v_w < 10^{-1}$, where the BAU has its maximum, may also prevent a quantitatively successful EWB. In all the models we considered we found a region of parameter space for which the deflagration is stable and the above conditions for ϕ_b/T and v_w are fulfilled.

We stress that the friction is very model-dependent, and current calculations have large errors which propagate to the wall velocity. For velocities close to the speed of sound, such $\mathcal{O}(1)$ factors may determine whether the wall propagates as a deflagration or a detonation. Similarly, for wall velocities close to the critical value, $\mathcal{O}(1)$ variations of the friction will determine the stability or instability of the deflagration. The calculation of the critical velocity is not easy either. We have used the analytic results of ref. [18], which were obtained using several approximations, such as the bag EOS and the assumption of planar walls. Nevertheless, the value of v_{crit} is less dependent on details of the specific model (i.e., it depends only on thermodynamical parameters). In the appendix we give a simple fit for v_{crit} as a function of the parameters $L/w_+(T_c)$ and T_n/T_c.

We also remark that we have used for our calculations a simple phenomenological model for the friction force. We have argued that this approximation should be good at least for the case of small wall velocities which are required for baryogenesis. The actual value of v_{crit} is possibly higher than our result. Hence, our calculation gives only a conservative lower bound for the velocity of a stable deflagration.

Acknowledgments

A Phase transition dynamics

A.1 Bubble nucleation and expansion

The bubble nucleation probability per unit volume per unit time is given by [80–82]

$$\Gamma_n(T) = A(T) e^{-S_3(T)/T}, \tag{A.1}$$

where $A(T) = [S_3(T)/(2\pi T)]^{3/2}$ and $S_3(T)$ is obtained by extremizing the three-dimensional instanton action

$$S_3[\phi] = 4\pi \int_0^\infty r^2 dr \left[\frac{1}{2} \left(\frac{d\phi}{dr} \right)^2 + V_T(\phi(r)) \right], \tag{A.2}$$

where $V_T(\phi)$ is defined in eq. (3.6). The variation of $S_3[\phi]$ gives an equation for the configuration of the nucleated bubble. The latter is assumed to be spherically symmetric, and its radial configuration $\phi_n(r)$ satisfies the boundary conditions $d\phi_n/dr|_{r=0} = 0$, $\lim_{r\to\infty} \phi_n(r) = 0$. We solve the equation for $\phi_n(r)$ iteratively by the overshoot-undershoot method (see ref. [76] for details).

The nucleation rate vanishes at $T = T_c$ and grows rapidly as T descends below T_c. At a temperature $T < T_c$, the probability of finding a bubble in a causal volume $V_c \sim (2/H)^3$ is given by

$$P(T) = \int_{T_c}^T \Gamma_n(T) V_c \frac{dt}{dT} dT. \tag{A.3}$$

The time-temperature relation is given by $dT/dt = -HT$, where the expansion rate is given by $H = \sqrt{8\pi G \rho_u(T)/3}$, with G the Newton's constant. We define as usual the nucleation temperature T_n at which nucleation effectively begins by the condition $P(T_n) = 1$. We compute T_n numerically from eqs. (A.1 -A.3).

A.2 Hydrodynamics

The equation for the wall can be obtained from the phenomenological equation for ϕ, which is similar to eq. (2.3), with the last term replaced by a phenomenological term proportional to $u^\mu \partial_\mu \phi$. The usual procedure is to consider the equation in the reference frame of the planar wall, multiply by $\partial\phi/\partial z$, where z is the coordinate perpendicular to the wall, and then integrate across the wall, taking into account the variation of the fluid variables. To perform the integration, either an ansatz for the wall profile is used or some approximations are needed. We shall use the result of [18], which uses linear approximations for the variations of quantities inside the wall. We have

$$p_u(T_u) - p_b(T_b) - \left\langle \frac{dp}{dT^2} \right\rangle (T_u^2 - T_b^2) - \eta \langle \gamma v \rangle = 0. \tag{A.4}$$

We also use the bag EOS,

$$p_u(T) = \frac{a}{3}T^4 - \frac{L}{4}, \quad p_b(T) = \left(\frac{a}{3} - \frac{L}{4T_c^4} \right) T^4, \tag{A.5}$$

where L is the latent heat and a is an effective radiation constant depending on the number of relativistic d.o.f. For the bag EOS, eq. (A.4) becomes

$$\frac{L}{4} \left(1 - \frac{T_u^2 T_b^2}{T_c^4} \right) = \eta \langle \gamma v \rangle. \tag{A.6}$$

The temperature T_b behind the wall is related to the temperature T_u in front of it through the equations for the discontinuity, eqs. (2.4). For the bag EOS we have

$$T_b^4 = \frac{v_u \gamma_u^2}{v_b \gamma_b^2 (1 - \bar{L})} T_u^4, \tag{A.7}$$

– 22 –

where $\bar{L} = L/(4aT_c^4/3) = L/w_u(T_c)$. The velocities v_u and v_b are related by [83]

$$v_u = \frac{1}{1+\alpha_u}\left[\frac{1}{6v_b} + \frac{v_b}{2} \pm \sqrt{\left(\frac{1}{6v_b} + \frac{v_b}{2}\right)^2 + \alpha_u^2 + \frac{2}{3}\alpha_u - \frac{1}{3}}\right],\qquad\text{(A.8)}$$

with $\alpha_u = L/\left(4aT_u^4\right) = (\bar{L}/3)(T_c/T_u)^4$.

We see that we have two kinds of solutions. Indeed, the $+$ sign in front of the square root in eq. (A.8) corresponds to detonations while the $-$ sign corresponds to deflagrations. For detonations we have $v_b < v_u$ while for deflagrations we have $v_b > v_u$. These solutions are further classified into weak, strong or Jouguet, depending on the relation of the outgoing velocity v_b with the speed of sound $c_s = 1/\sqrt{3}$. For weak deflagrations we have $v_b < c_s$.

The fluid profiles away from the wall are quite simple for a planar interface. For a weak deflagration we can only have constant fluid velocities. In the reference frame of the bubble center, the velocity profile is the following. Inside the bubble the fluid is at rest (in the reference frame of the wall, this gives the condition $v_b = v_w$). In front of the wall we have a constant fluid velocity $\tilde{v}_u > 0$ (in the wall frame, this inequality transforms into the deflagration relation $v_u < v_b$). The boundary condition of an unperturbed fluid far in front of the wall is fulfilled by a jump of the fluid velocity from $\tilde{v}_u$ to 0 at a certain point. Such a discontinuity in the fluid profile is called a shock front.

The shock discontinuity is also determined by applying eqs. (2.4) to the shock front, where the EOS is now the same in both sides of the interface. It turns out that the shock front moves supersonically. The region between the bubble wall and the shock front is reheated, i.e., the temperature T_u is higher than the nucleation temperature T_n. We have

$$\frac{\sqrt{3}\left(T_u^4 - T_n^4\right)}{\sqrt{\left(3T_u^4 + T_n^4\right)\left(3T_n^4 + T_u^4\right)}} = \frac{v_b - v_u}{1 - v_u v_b}.\qquad\text{(A.9)}$$

Using the relations (A.7)–(A.8), the two equations (A.6) and (A.9) can be readily solved to obtain v_w as a function of η and T_n.

B The critical velocity

Using the relations (A.7)–(A.9) in eq. (2.8), we obtain the equation for the critical velocity v_{crit} as a function of T_n/T_c and $\bar{L}$. The solution for v_{crit} is plotted in figure 7 (solid lines) as a function of $\bar{L}$ for different values of T_n/T_c. Technically, solving eq. (2.8) becomes difficult in some cases due to the divergence of the quantity β as the product $T_u T_b$ approaches T_c^2. This happens for instance for high values of the latent heat, since the reheating in front of the wall may cause T_u to exceed T_c. As can be seen from eq. (A.6), the exact limit cannot be reached and we always have $T_u T_b < T_c^2$. As a consequence, there is always a critical velocity.

In the case of small supercooling and small latent heat, the wall velocity is generally small, since we have $\eta v_w \simeq L(1 - T_u/T_c)$. In this limit we also have $T_b \simeq T_u$ and $v_b \simeq v_u$, and we have a simple expression for v_{crit} as a function of T_u [18],

$$v_{\text{crit}}^2 \simeq (1 + \bar{L})\left(1 - \frac{T_u}{T_c}\right).\qquad\text{(B.1)}$$
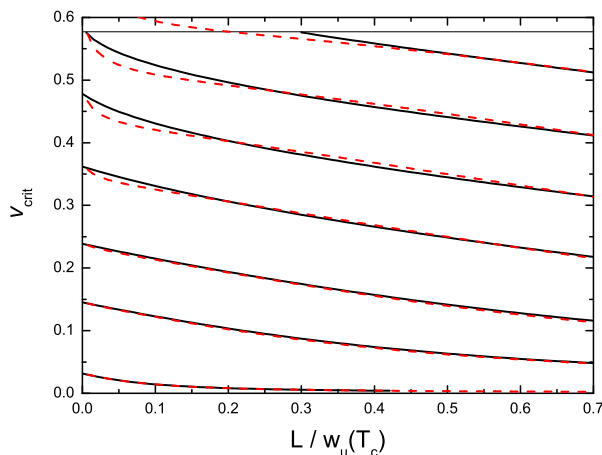
Figure 7. The critical velocity (solid lines) and the fit (dashed lines) as functions of the parameter $\bar{L}$ for several amounts of supercooling. From bottom to top we have $T_n/T_c = 0.999$, 0.98, 0.95, 0.9, 0.85, 0.8 and 0.75. The horizontal line indicates the value $c_s = 1/\sqrt{3}$.

On the other hand, the temperature T_u of the reheated plasma in front of the wall depends on v_w. In the present approximation we have $T_u/T_c \simeq T_n/T_c + (\bar{L}/\sqrt{3}v_w)$. Hence, for $v_w = v_{\mathrm{crit}}$ eq. (B.1) gives a quadratic equation. The solution is

$$v_{\mathrm{crit}} \simeq \frac{\bar{L}(1 + \bar{L})}{2\sqrt{3}} \left[\sqrt{1 + \frac{12}{\bar{L}^2(1 + \bar{L})} \left(1 - \frac{T_n}{T_c} \right)} - 1 \right]. \tag{B.2}$$

This simple approximation underestimates the value of the critical velocity. It becomes exact in the limit $T_n \to T_c$, but only gives a good estimation for small amounts of supercooling. For instance, for $T_n/T_c > 0.98$ the error is less than a 5%, while for $T_n/T_c = 0.9$ the actual value of the critical velocity is about a 15% higher than the approximation (B.2).

Nevertheless, a slight modification of eq. (B.2) provides a good fit,

$$v_{\mathrm{crit}} \simeq \frac{\bar{L}(1 + \bar{L})}{2\sqrt{3}} \left[\sqrt{1 + \frac{12}{\bar{L}^{2+\varepsilon}(1 + a\bar{L})} \left(1 - \frac{T_n}{T_c} \right)} - 1 \right], \tag{B.3}$$

with $\varepsilon = 0.5(1 - T_n/T_c)$ and $a = 1 - 2.7(1 - T_n/T_c)$. The error of this approximation is less than a 5% for $0.75 < T_n/T_c < 1$ and in all the range $0 < \bar{L} < 1$ (see figure 7).

References

[1] D.E. Morrissey and M.J. Ramsey-Musolf, *Electroweak baryogenesis*, *New J. Phys.* **14** (2012) 125003 [arXiv:1206.2942].

[2] M. Kamionkowski, A. Kosowsky and M.S. Turner, *Gravitational radiation from first order phase transitions*, *Phys. Rev.* **D 49** (1994) 2837 [astro-ph/9310044] [INSPIRE].

[3] J.M. Cline and K. Kainulainen, *A New source for electroweak baryogenesis in the MSSM*, *Phys. Rev. Lett.* **85** (2000) 5519 [hep-ph/0002272] [INSPIRE].

[4] J.M. Cline, M. Joyce and K. Kainulainen, *Supersymmetric electroweak baryogenesis*, *JHEP* **07** (2000) 018 [hep-ph/0006119] [INSPIRE].

[5] M. Carena, J.M. Moreno, M. Quirós, M. Seco and C.E.M. Wagner, *Supersymmetric CP-violating currents and electroweak baryogenesis*, *Nucl. Phys.* **B 599** (2001) 158 [`hep-ph/0011055`] [ɪɴSPIRE].

[6] M. Joyce, T. Prokopec and N. Turok, *Nonlocal electroweak baryogenesis. Part 2: The Classical regime*, *Phys. Rev.* **D 53** (1996) 2958 [`hep-ph/9410282`] [ɪɴSPIRE].

[7] L.D. Landau and E.M. Lifshitz, *Fluid Mechanics*, Pergamon Press, New York U.S.A. (1989).

[8] M. Gyulassy, K. Kajantie, H. Kurki-Suonio and L.D. McLerran, *Deflagrations and Detonations as a Mechanism of Hadron Bubble Growth in Supercooled Quark Gluon Plasma*, *Nucl. Phys.* **B 237** (1984) 477 [ɪɴSPIRE].

[9] K. Enqvist, J. Ignatius, K. Kajantie and K. Rummukainen, *Nucleation and bubble growth in a first order cosmological electroweak phase transition*, *Phys. Rev.* **D 45** (1992) 3415 [ɪɴSPIRE].

[10] H. Kurki-Suonio, *Deflagration Bubbles in the Quark-Hadron Phase Transition*, *Nucl. Phys.* **B 255** (1985) 231 [ɪɴSPIRE].

[11] K. Kajantie and H. Kurki-Suonio, *Bubble Growth and Droplet Decay in the Quark-Hadron Phase Transition in the Early Universe*, *Phys. Rev.* **D 34** (1986) 1719 [ɪɴSPIRE].

[12] J. Ignatius, K. Kajantie, H. Kurki-Suonio and M. Laine, *The growth of bubbles in cosmological phase transitions*, *Phys. Rev.* **D 49** (1994) 3854 [`astro-ph/9309059`] [ɪɴSPIRE].

[13] H. Kurki-Suonio and M. Laine, *Supersonic deflagrations in cosmological phase transitions*, *Phys. Rev.* **D 51** (1995) 5431 [`hep-ph/9501216`] [ɪɴSPIRE].

[14] H. Kurki-Suonio and M. Laine, *On bubble growth and droplet decay in cosmological phase transitions*, *Phys. Rev.* **D 54** (1996) 7163 [`hep-ph/9512202`] [ɪɴSPIRE].

[15] B. Link, *Deflagration instability in the quark-hadron phase transition*, *Phys. Rev. Lett.* **68** (1992) 2425 [ɪɴSPIRE].

[16] P.Y. Huet, K. Kajantie, R.G. Leigh, B.-H. Liu and L.D. McLerran, *Hydrodynamic stability analysis of burning bubbles in electroweak theory and in QCD*, *Phys. Rev.* **D 48** (1993) 2477 [`hep-ph/9212224`] [ɪɴSPIRE].

[17] P.C. Fragile and P. Anninos, *Hydrodynamic stability of cosmological quark hadron phase transitions*, *Phys. Rev.* **D 67** (2003) 103010 [`gr-qc/0303018`] [ɪɴSPIRE].

[18] A. Megevand and F.A. Membiela, *Stability of cosmological deflagration fronts*, *Phys. Rev.* **D 89** (2014) 103507 [`arXiv:1311.2453`] [ɪɴSPIRE].

[19] M. Dine, R.G. Leigh, P.Y. Huet, A.D. Linde and D.A. Linde, *Towards the theory of the electroweak phase transition*, *Phys. Rev.* **D 46** (1992) 550 [`hep-ph/9203203`] [ɪɴSPIRE].

[20] B.-H. Liu, L.D. McLerran and N. Turok, *Bubble nucleation and growth at a baryon number producing electroweak phase transition*, *Phys. Rev.* **D 46** (1992) 2668 [ɪɴSPIRE].

[21] G.D. Moore and T. Prokopec, *How fast can the wall move? A Study of the electroweak phase transition dynamics*, *Phys. Rev.* **D 52** (1995) 7182 [`hep-ph/9506475`] [ɪɴSPIRE].

[22] P. John and M.G. Schmidt, *Do stops slow down electroweak bubble walls?*, *Nucl. Phys.* **B 598** (2001) 291 [*Erratum ibid.* **B 648** (2003) 449-452] [`hep-ph/0002050`] [ɪɴSPIRE].

[23] G.D. Moore, *Electroweak bubble wall friction: Analytic results*, *JHEP* **03** (2000) 006 [`hep-ph/0001274`] [ɪɴSPIRE].

[24] G. Sigl, A.V. Olinto and K. Jedamzik, *Primordial magnetic fields from cosmological first order phase transitions*, *Phys. Rev.* **D 55** (1997) 4582 [`astro-ph/9610201`] [ɪɴSPIRE].

[25] N. Turok, *Electroweak bubbles: Nucleation and growth*, *Phys. Rev. Lett.* **68** (1992) 1803 [ɪɴSPIRE].

[26] S.Y. Khlebnikov, *Fluctuation-dissipation formula for bubble wall velocity*, *Phys. Rev.* **D 46** (1992) 3223 [INSPIRE].

[27] P.B. Arnold, *One loop fluctuation-dissipation formula for bubble wall velocity*, *Phys. Rev.* **D 48** (1993) 1539 [hep-ph/9302258] [INSPIRE].

[28] G.D. Moore and T. Prokopec, *Bubble wall velocity in a first order electroweak phase transition*, *Phys. Rev. Lett.* **75** (1995) 777 [hep-ph/9503296] [INSPIRE].

[29] A. Mégevand, *Friction forces on phase transition fronts*, *JCAP* **07** (2013) 045 [arXiv:1303.4233] [INSPIRE].

[30] D. Bödeker and G.D. Moore, *Can electroweak bubble walls run away?*, *JCAP* **05** (2009) 009 [arXiv:0903.4099] [INSPIRE].

[31] T. Konstandin, G. Nardini and I. Rues, *From Boltzmann equations to steady wall velocities*, *JCAP* **09** (2014) 028 [arXiv:1407.3132] [INSPIRE].

[32] A. Mégevand and A.D. Sánchez, *Analytic approach to the motion of cosmological phase transition fronts*, *Nucl. Phys.* **B 865** (2012) 217 [arXiv:1206.2339] [INSPIRE].

[33] A. Mégevand and A.D. Sánchez, *Detonations and deflagrations in cosmological phase transitions*, *Nucl. Phys.* **B 820** (2009) 47 [arXiv:0904.1753] [INSPIRE].

[34] J.R. Espinosa, T. Konstandin, J.M. No and G. Servant, *Energy Budget of Cosmological First-order Phase Transitions*, *JCAP* **06** (2010) 028 [arXiv:1004.4187] [INSPIRE].

[35] L. Leitao and A. Mégevand, *Hydrodynamics of phase transition fronts and the speed of sound in the plasma*, *Nucl. Phys.* **B 891** (2015) 159 [arXiv:1410.3875] [INSPIRE].

[36] T. Konstandin and J.M. No, *Hydrodynamic obstruction to bubble expansion*, *JCAP* **02** (2011) 008 [arXiv:1011.3735] [INSPIRE].

[37] M. Abney, *Hydrodynamic detonation instability in electroweak and QCD phase transitions*, *Phys. Rev.* **D 49** (1994) 1777 [astro-ph/9305021] [INSPIRE].

[38] L. Rezzolla, *Stability of cosmological detonation front*, *Phys. Rev.* **D 54** (1996) 1345 [astro-ph/9605033] [INSPIRE].

[39] A. Mégevand and F.A. Membiela, *Stability of cosmological detonation fronts*, *Phys. Rev.* **D 89** (2014) 103503 [arXiv:1402.5791] [INSPIRE].

[40] D.J.H. Chung, A.J. Long and L.-T. Wang, *125 GeV Higgs boson and electroweak phase transition model classes*, *Phys. Rev.* **D 87** (2013) 023509 [arXiv:1209.1819] [INSPIRE].

[41] M. Carena, G. Nardini, M. Quirós and C.E.M. Wagner, *MSSM Electroweak Baryogenesis and LHC Data*, *JHEP* **02** (2013) 001 [arXiv:1207.6330] [INSPIRE].

[42] A. Katz and M. Perelstein, *Higgs Couplings and Electroweak Phase Transition*, *JHEP* **07** (2014) 108 [arXiv:1401.1827] [INSPIRE].

[43] M. Carena, A. Mégevand, M. Quirós and C.E.M. Wagner, *Electroweak baryogenesis and new TeV fermions*, *Nucl. Phys.* **B 716** (2005) 319 [hep-ph/0410352] [INSPIRE].

[44] M. Quirós, *Finite temperature field theory and phase transitions*, hep-ph/9901312 [INSPIRE].

[45] G.W. Anderson and L.J. Hall, *The Electroweak phase transition and baryogenesis*, *Phys. Rev.* **D 45** (1992) 2685 [INSPIRE].

[46] A. Mégevand, *First order cosmological phase transitions in the radiation dominated era*, *Phys. Rev.* **D 69** (2004) 103521 [hep-ph/0312305] [INSPIRE].

[47] A. Mégevand and A.D. Sánchez, *Velocity of electroweak bubble walls*, *Nucl. Phys.* **B 825** (2010) 151 [arXiv:0908.3663] [INSPIRE].

[48] S.J. Huber and M. Sopena, *The bubble wall velocity in the minimal supersymmetric light stop scenario*, *Phys. Rev.* **D 85** (2012) 103507 [`arXiv:1112.1888`] [ɪɴSPIRE].

[49] J. Choi and R.R. Volkas, *Real Higgs singlet and the electroweak phase transition in the Standard Model*, *Phys. Lett.* **B 317** (1993) 385 [`hep-ph/9308234`] [ɪɴSPIRE].

[50] J.R. Espinosa and M. Quirós, *The Electroweak phase transition with a singlet*, *Phys. Lett.* **B 305** (1993) 98 [`hep-ph/9301285`] [ɪɴSPIRE].

[51] M. Carena, M. Quirós and C.E.M. Wagner, *Opening the window for electroweak baryogenesis*, *Phys. Lett.* **B 380** (1996) 81 [`hep-ph/9603420`] [ɪɴSPIRE].

[52] J.R. Espinosa, *Dominant two loop corrections to the MSSM finite temperature effective potential*, *Nucl. Phys.* **B 475** (1996) 273 [`hep-ph/9604320`] [ɪɴSPIRE].

[53] M. Carena, M. Quirós and C.E.M. Wagner, *Electroweak baryogenesis and Higgs and stop searches at LEP and the Tevatron*, *Nucl. Phys.* **B 524** (1998) 3 [`hep-ph/9710401`] [ɪɴSPIRE].

[54] M. Carena, G. Nardini, M. Quirós and C.E.M. Wagner, *The Baryogenesis Window in the MSSM*, *Nucl. Phys.* **B 812** (2009) 243 [`arXiv:0809.3760`] [ɪɴSPIRE].

[55] S.W. Ham, Y.S. Jeong and S.K. Oh, *Electroweak phase transition in an extension of the standard model with a real Higgs singlet*, *J. Phys.* **G 31** (2005) 857 [`hep-ph/0411352`] [ɪɴSPIRE].

[56] A. Ahriche, *What is the criterion for a strong first order electroweak phase transition in singlet models?*, *Phys. Rev.* **D 75** (2007) 083522 [`hep-ph/0701192`] [ɪɴSPIRE].

[57] S. Profumo, M.J. Ramsey-Musolf and G. Shaughnessy, *Singlet Higgs phenomenology and the electroweak phase transition*, *JHEP* **08** (2007) 010 [`arXiv:0705.2425`] [ɪɴSPIRE].

[58] A. Ashoorioon and T. Konstandin, *Strong electroweak phase transitions without collider traces*, *JHEP* **07** (2009) 086 [`arXiv:0904.0353`] [ɪɴSPIRE].

[59] J.R. Espinosa, T. Konstandin and F. Riva, *Strong Electroweak Phase Transitions in the Standard Model with a Singlet*, *Nucl. Phys.* **B 854** (2012) 592 [`arXiv:1107.5441`] [ɪɴSPIRE].

[60] J.M. Cline and K. Kainulainen, *Electroweak baryogenesis and dark matter from a singlet Higgs*, *JCAP* **01** (2013) 012 [`arXiv:1210.4196`] [ɪɴSPIRE].

[61] M. Pietroni, *The Electroweak phase transition in a nonminimal supersymmetric model*, *Nucl. Phys.* **B 402** (1993) 27 [`hep-ph/9207227`] [ɪɴSPIRE].

[62] A.T. Davies, C.D. Froggatt and R.G. Moorhouse, *Electroweak baryogenesis in the next-to-minimal supersymmetric model*, *Phys. Lett.* **B 372** (1996) 88 [`hep-ph/9603388`] [ɪɴSPIRE].

[63] S.J. Huber and M.G. Schmidt, *Electroweak baryogenesis: Concrete in a SUSY model with a gauge singlet*, *Nucl. Phys.* **B 606** (2001) 183 [`hep-ph/0003122`] [ɪɴSPIRE].

[64] A. Menon, D.E. Morrissey and C.E.M. Wagner, *Electroweak baryogenesis and dark matter in the NMSSM*, *Phys. Rev.* **D 70** (2004) 035005 [`hep-ph/0404184`] [ɪɴSPIRE].

[65] X.-m. Zhang, *Operators analysis for Higgs potential and cosmological bound on Higgs mass*, *Phys. Rev.* **D 47** (1993) 3065 [`hep-ph/9301277`] [ɪɴSPIRE].

[66] S.W. Ham and S.K. Oh, *Electroweak phase transition in the standard model with a dimension-six Higgs operator at one-loop level*, *Phys. Rev.* **D 70** (2004) 093007 [`hep-ph/0408324`] [ɪɴSPIRE].

[67] C. Grojean, G. Servant and J.D. Wells, *First-order electroweak phase transition in the standard model with a low cutoff*, *Phys. Rev.* **D 71** (2005) 036001 [`hep-ph/0407019`] [ɪɴSPIRE].

[68] B. Grinstein and M. Trott, *Electroweak Baryogenesis with a Pseudo-Goldstone Higgs*, *Phys. Rev.* **D 78** (2008) 075022 [`arXiv:0806.1971`] [ɪɴSPIRE].

[69] C. Delaunay, C. Grojean and J.D. Wells, *Dynamics of Non-renormalizable Electroweak Symmetry Breaking*, *JHEP* **04** (2008) 029 [`arXiv:0711.2511`] [ɪɴSPIRE].

[70] J.R. Espinosa and M. Quirós, *Novel Effects in Electroweak Breaking from a Hidden Sector*, *Phys. Rev.* **D 76** (2007) 076004 [`hep-ph/0701145`] [ɪɴSPIRE].

[71] J.R. Espinosa, T. Konstandin, J.M. No and M. Quirós, *Some Cosmological Implications of Hidden Sectors*, *Phys. Rev.* **D 78** (2008) 123528 [`arXiv:0809.3215`] [ɪɴSPIRE].

[72] L. Leitao, A. Mégevand and A.D. Sánchez, *Gravitational waves from the electroweak phase transition*, *JCAP* **10** (2012) 024 [`arXiv:1205.3070`] [ɪɴSPIRE].

[73] K. Freese and F.C. Adams, *Hadron Bubble Evolution: Voyage Into the Quark Sea*, *Phys. Rev.* **D 41** (1990) 2449 [ɪɴSPIRE].

[74] E. Suhonen, *The Quark-Hadron Phase Transition in the Early Universe*, *Phys. Lett.* **B 119** (1982) 81 [ɪɴSPIRE].

[75] E. Witten, *Cosmic Separation of Phases*, *Phys. Rev.* **D 30** (1984) 272 [ɪɴSPIRE].

[76] A. Mégevand and A.D. Sánchez, *Supercooling and phase coexistence in cosmological phase transitions*, *Phys. Rev.* **D 77** (2008) 063519 [`arXiv:0712.1031`] [ɪɴSPIRE].

[77] A.F. Heckler, *The Effects of electroweak phase transition dynamics on baryogenesis and primordial nucleosynthesis*, *Phys. Rev.* **D 51** (1995) 405 [`astro-ph/9407064`] [ɪɴSPIRE].

[78] A. Mégevand, *Effect of reheating on electroweak baryogenesis*, *Phys. Rev.* **D 64** (2001) 027303 [`hep-ph/0011019`] [ɪɴSPIRE].

[79] A. Mégevand and F. Astorga, *Generation of baryon inhomogeneities in the electroweak phase transition*, *Phys. Rev.* **D 71** (2005) 023502 [`hep-ph/0409321`] [ɪɴSPIRE].

[80] I. Affleck, *Quantum Statistical Metastability*, *Phys. Rev. Lett.* **46** (1981) 388 [ɪɴSPIRE].

[81] A.D. Linde, *Decay of the False Vacuum at Finite Temperature*, *Nucl. Phys.* **B 216** (1983) 421 [*Erratum ibid.* **B 223** (1983) 544] [ɪɴSPIRE].

[82] A.D. Linde, *Fate of the False Vacuum at Finite Temperature: Theory and Applications*, *Phys. Lett.* **B 100** (1981) 37 [ɪɴSPIRE].

[83] P.J. Steinhardt, *Relativistic Detonation Waves and Bubble Growth in False Vacuum Decay*, *Phys. Rev.* **D 25** (1982) 2074 [ɪɴSPIRE].